Supporting Information for "Revisiting western United States hydroclimate during the last deglaciation"

Minmin Fu[1]

[1]Department of Earth and Planetary Sciences, Yale University, New Haven, CT, USA

Contents of this file

1. Figures S1 to S12

2. References

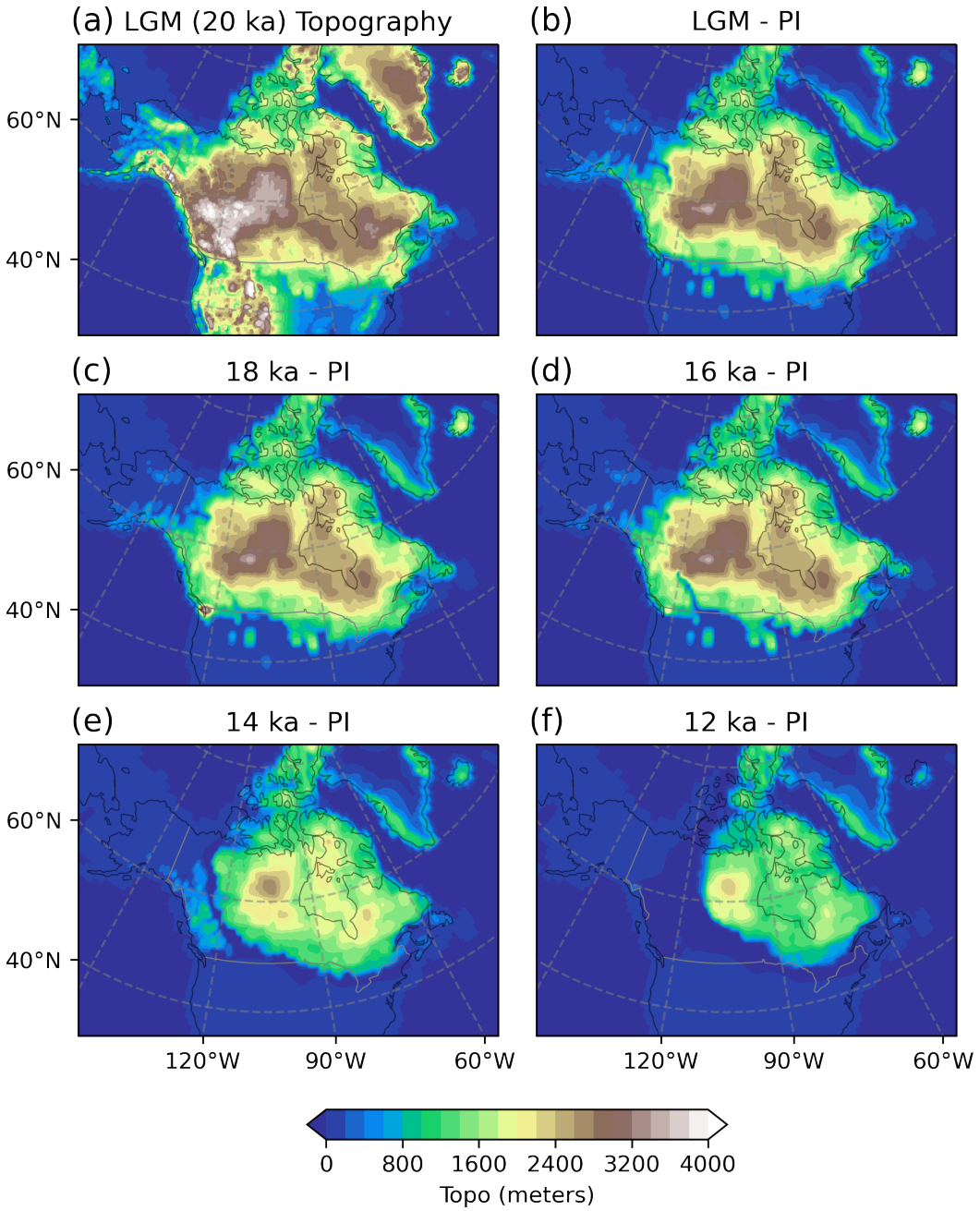

Figure S1. (a) Ice-sheet topography (meters) during the LGM (20 ka) from the ICE-6G reconstruction (Peltier et al., 2015). (b) Difference in ice-sheet topography between LGM and preindustrial. (c–f) As in (b), but differences from preindustrial for 18, 16, 14, and 12 ka, respectively.

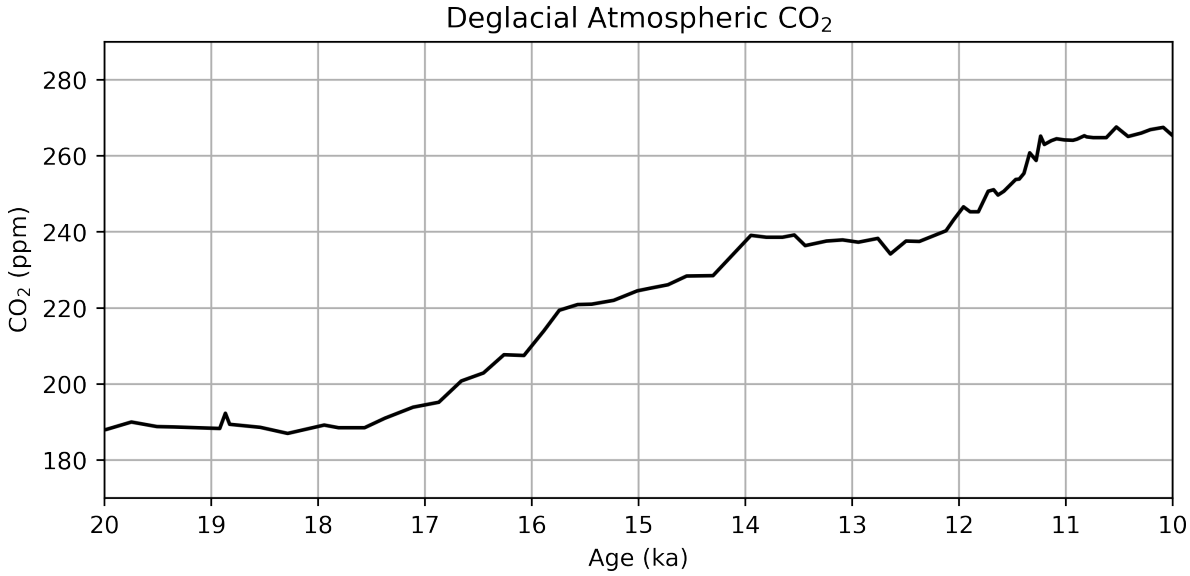

Figure S2. Atmospheric CO_2 concentration during the last deglaciation (Lüthi et al., 2008; Monnin et al., 2001).

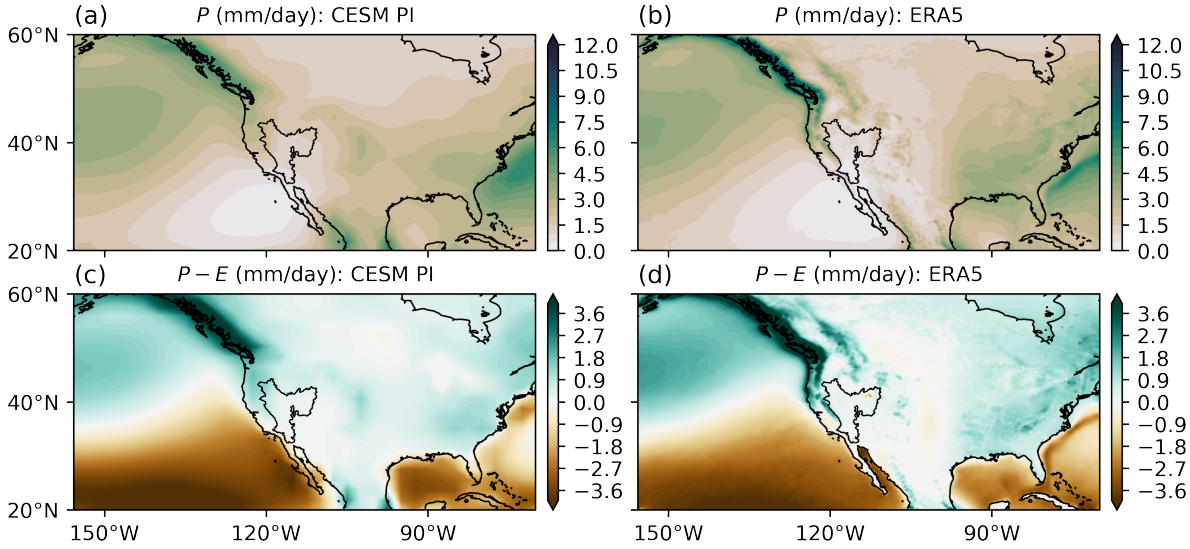

Figure S3. (a) Annual-mean precipitation rate for the preindustrial CESM 1.2 simulation. (b) As in (a), but for ERA5 reanalysis. (c) Annual-mean precipitation minus evaporation ($P - E$) for preindustrial CESM 1.2. (d) As in (c), but for ERA5 reanalysis.

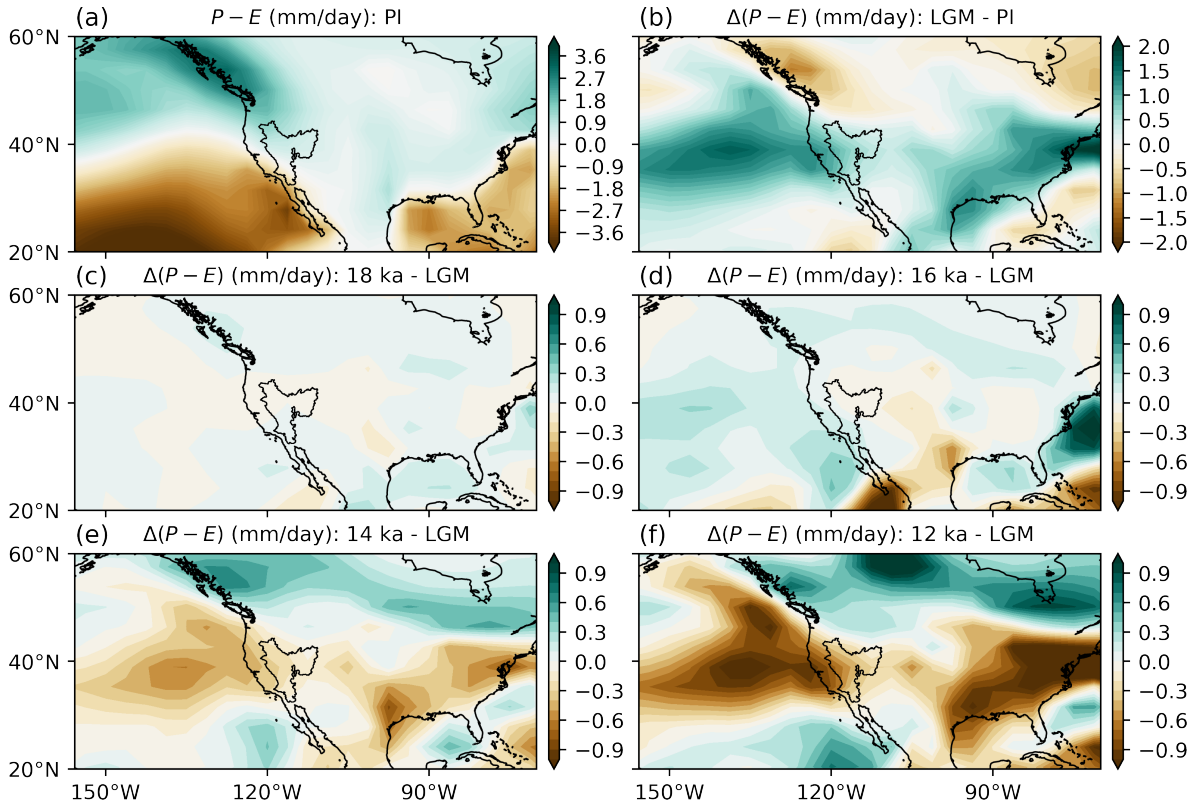

Figure S4. Maps of annual-mean $P-E$ in TraCE-21ka. (a) $P-E$ in the preindustrial simulation. (b) Difference in $P-E$ between LGM (20 ka) and PI. (c) Difference between 18 ka and LGM. (d–f) As in (c), but for differences between 16, 14, and 12 ka from LGM respectively.

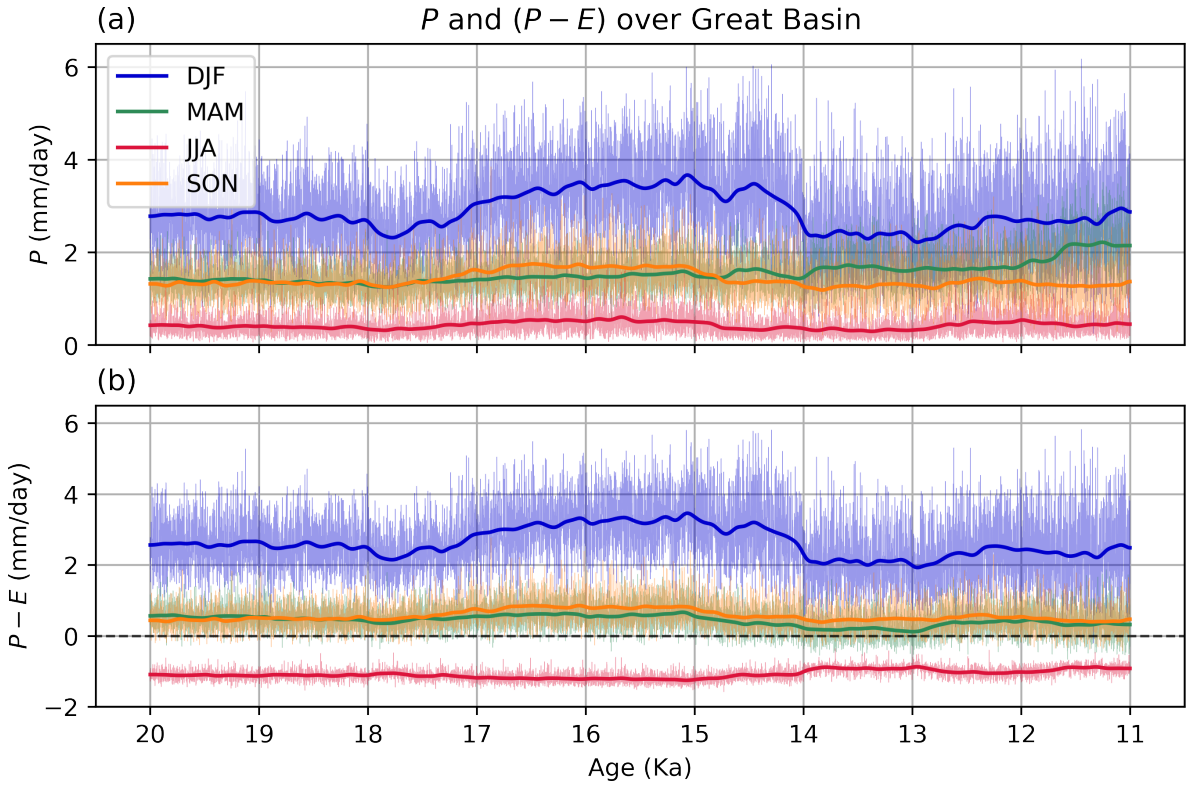

Figure S5. Hydrological cycle during deglaciation, averaged over the Great Basin watershed for individual seasons in iTraCE. (a) Seasonal mean precipitation (P), from 20 ka to 11 ka shown in the thin curve. The thick curve shows the long term trend, with a Gaussian filter ($\sigma = 100$) applied. (b) As in panel (a), but for precipitation minus evaporation ($P - E$).

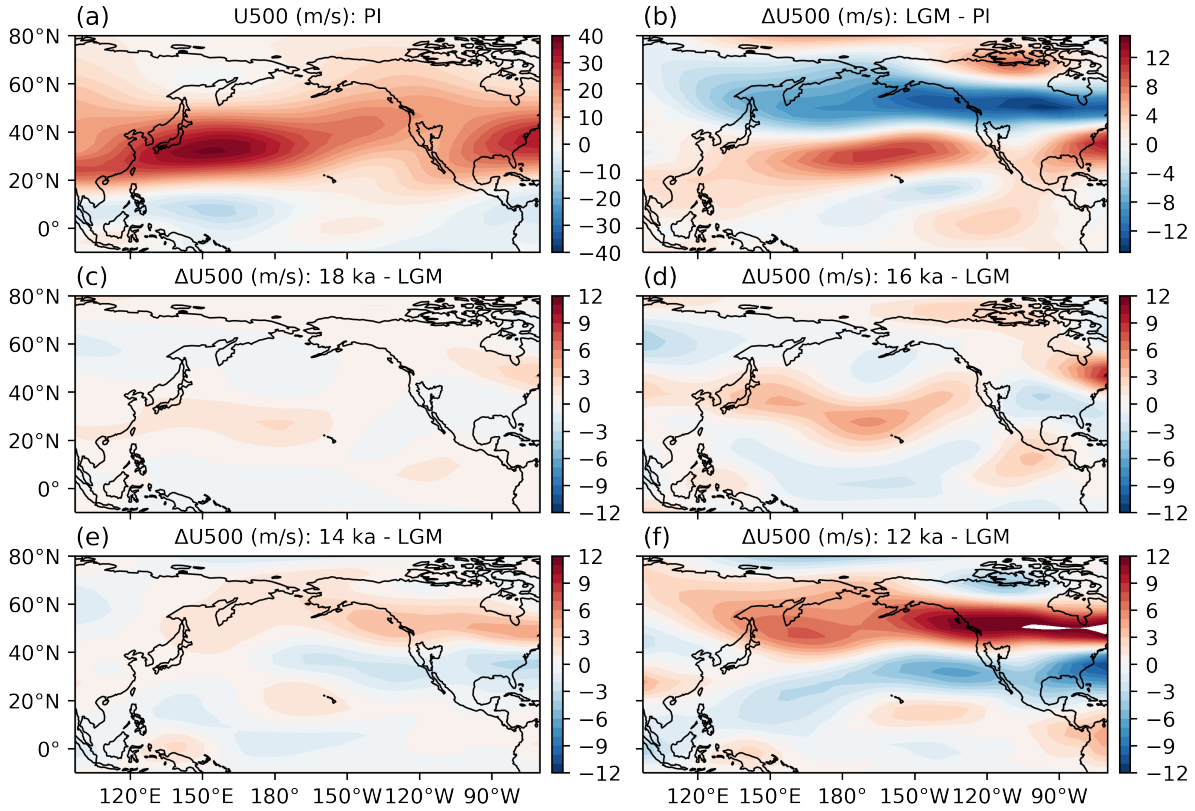

Figure S6. Winter-mean (DJF) atmospheric circulation over the North Pacific in TraCE-21ka. (a) Zonal velocity at 500 hPa (U500; m/s) in the preindustrial simulation. (b) Difference in U500 between LGM (20 ka) and PI. (c) Difference between 18 ka and LGM. (d–f) As in (c), but for differences between 16, 14, and 12 ka from LGM respectively.

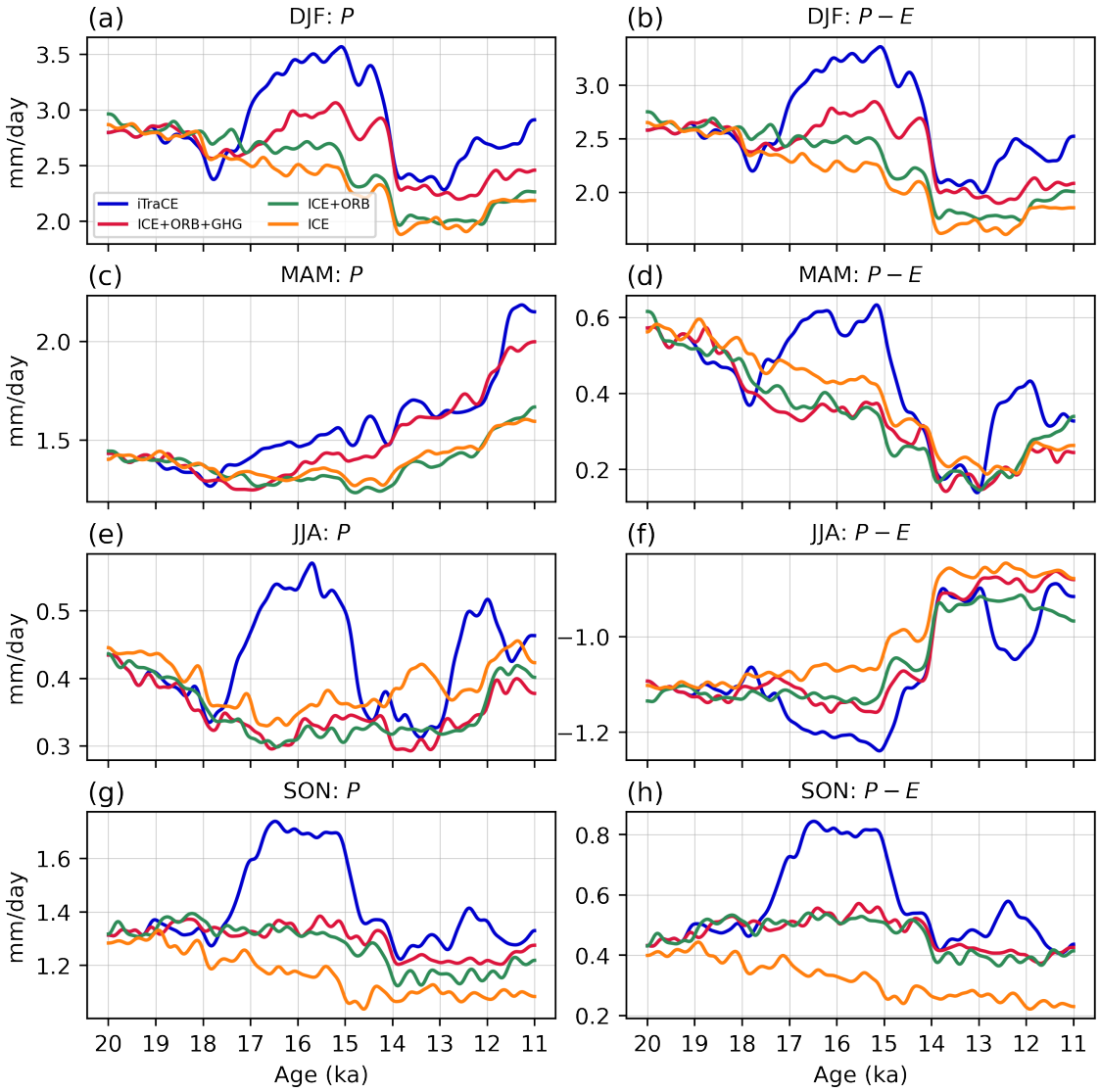

Figure S7. Hydrological cycle over the Great Basin watershed in additive forcing experiments, for individual seasons in iTraCE. (a) Long term trend in DJF-mean precipitation (P), from 20 ka to 11 ka, with four major forcing factors applied additively. A Gaussian filter ($\sigma = 100$) has been applied to all curves. (b) As in panel (a), but for precipitation minus evaporation ($P - E$). (c,d) As in (a,b), but for MAM. (e,f) As in (a,b), but for JJA. (g,h) As in (a,b), but for SON.

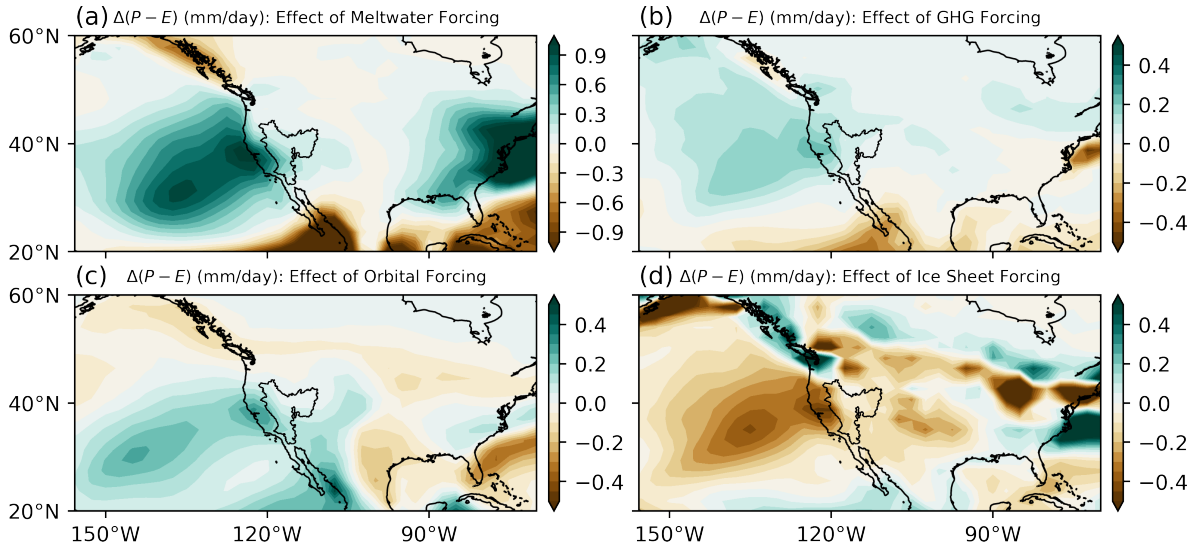

Figure S8. Difference in annual-mean $P - E$ between 16 ka and LGM in iTraCE, decomposed into contributions from various forcing factors. (a) Difference in $P - E$ from meltwater forcing (16 ka - 16 ka_ICE+ORB+GHG). (b) Effect of greenhouse gas forcing (16 ka_ICE+ORB+GHG - 16 ka_ICE+ORB). (c) Effect of orbital forcing (16 ka_ICE+ORB - 16 ka_ICE). (d) Effect of changing ice sheets and bathymetry (16 ka_ice - LGM).

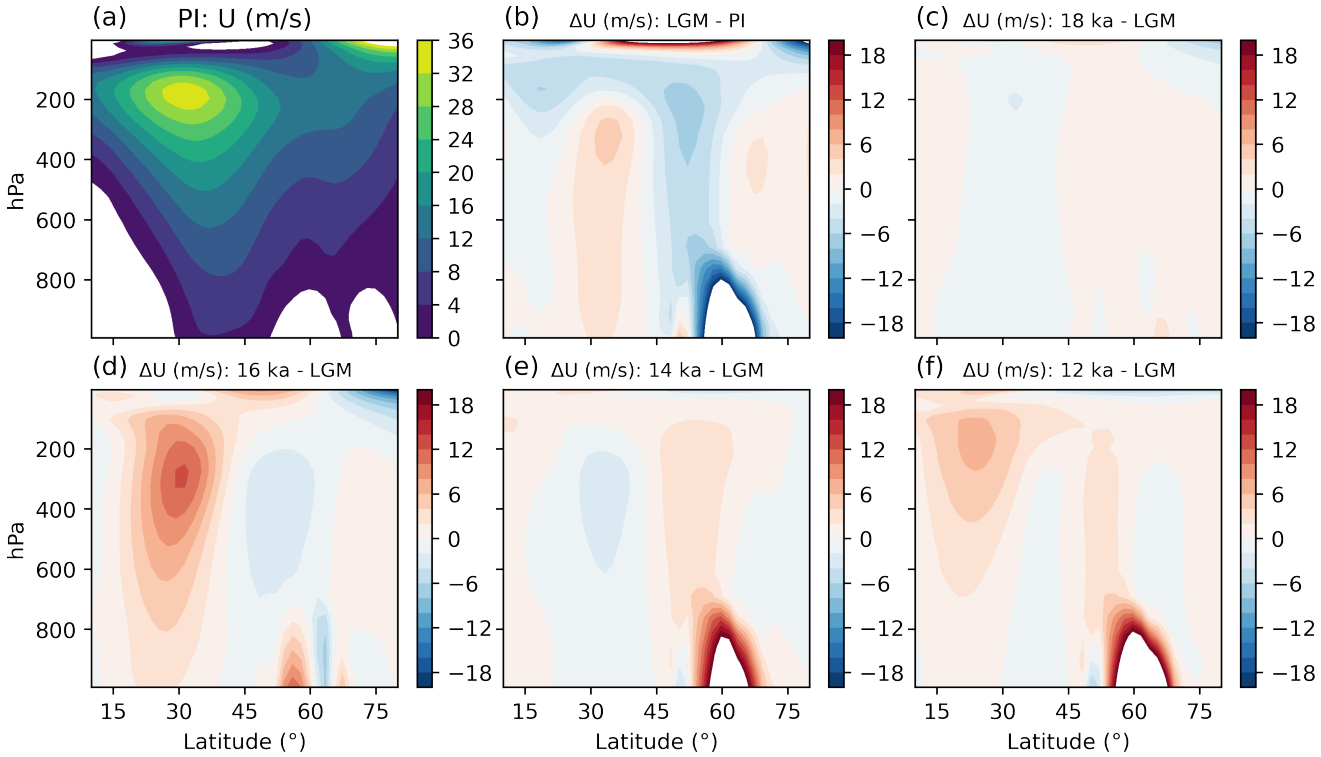

Figure S9. Winter-mean (DJF) zonal winds averaged over the eastern North Pacific (120°W–150°W) in iTraCE. (a) U (m/s) in the preindustrial simulation. (b) Difference between and LGM and PI. (c) Difference between 18 ka and LGM. (d–f) As in (c), but differences from LGM for 16 ka, 14 ka, and 12 ka, respectively.

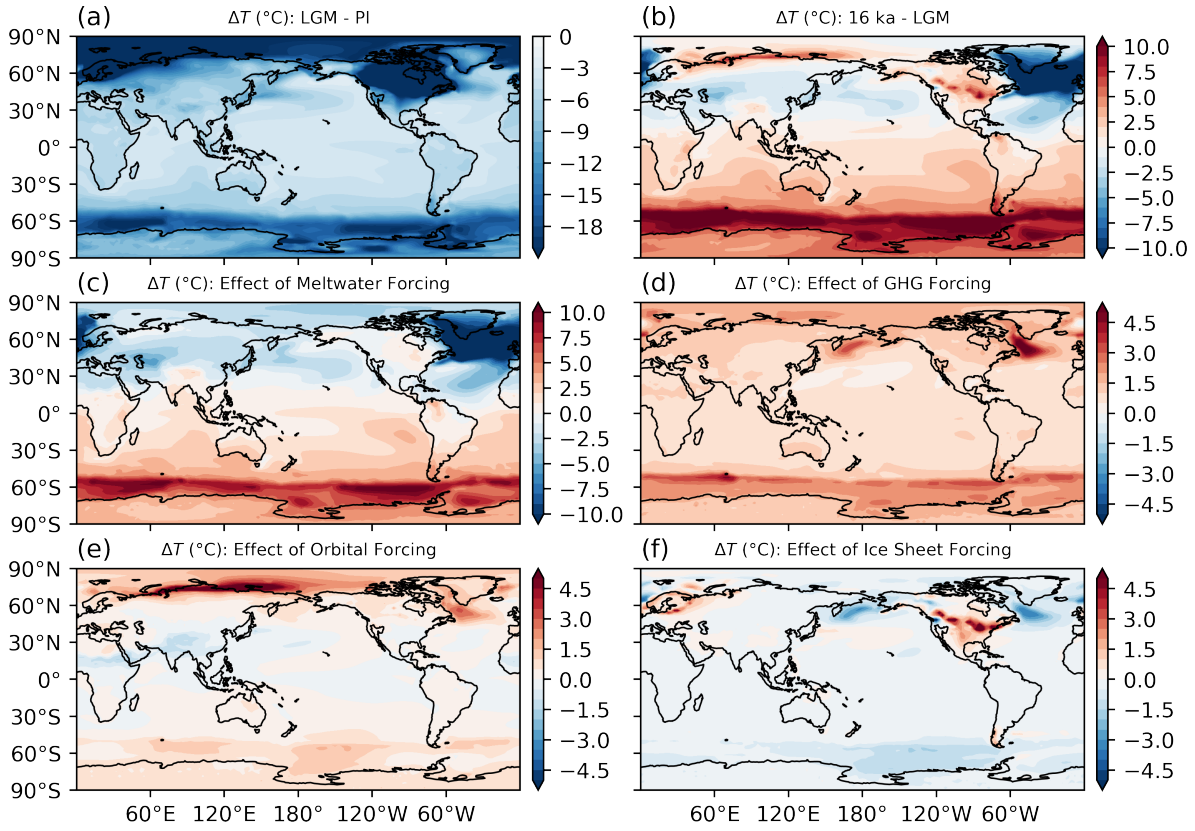

Figure S10. (a) Annual-mean surface temperature differences between LGM and PI in iTraCE. (b) Difference between 16 ka and LGM. (c) Difference in surface temperature from meltwater forcing (16 ka - 16 ka_ICE+ORB+GHG). (d) Difference from greenhouse gas forcing (16 ka_ICE+ORB+GHG - 16 ka_ICE+ORB). (e) Difference from insolation forcing (16 ka_ICE+ORB - 16 ka_ICE). (f) Difference from changing ice sheets and bathymetry (16 ka_ICE - LGM).

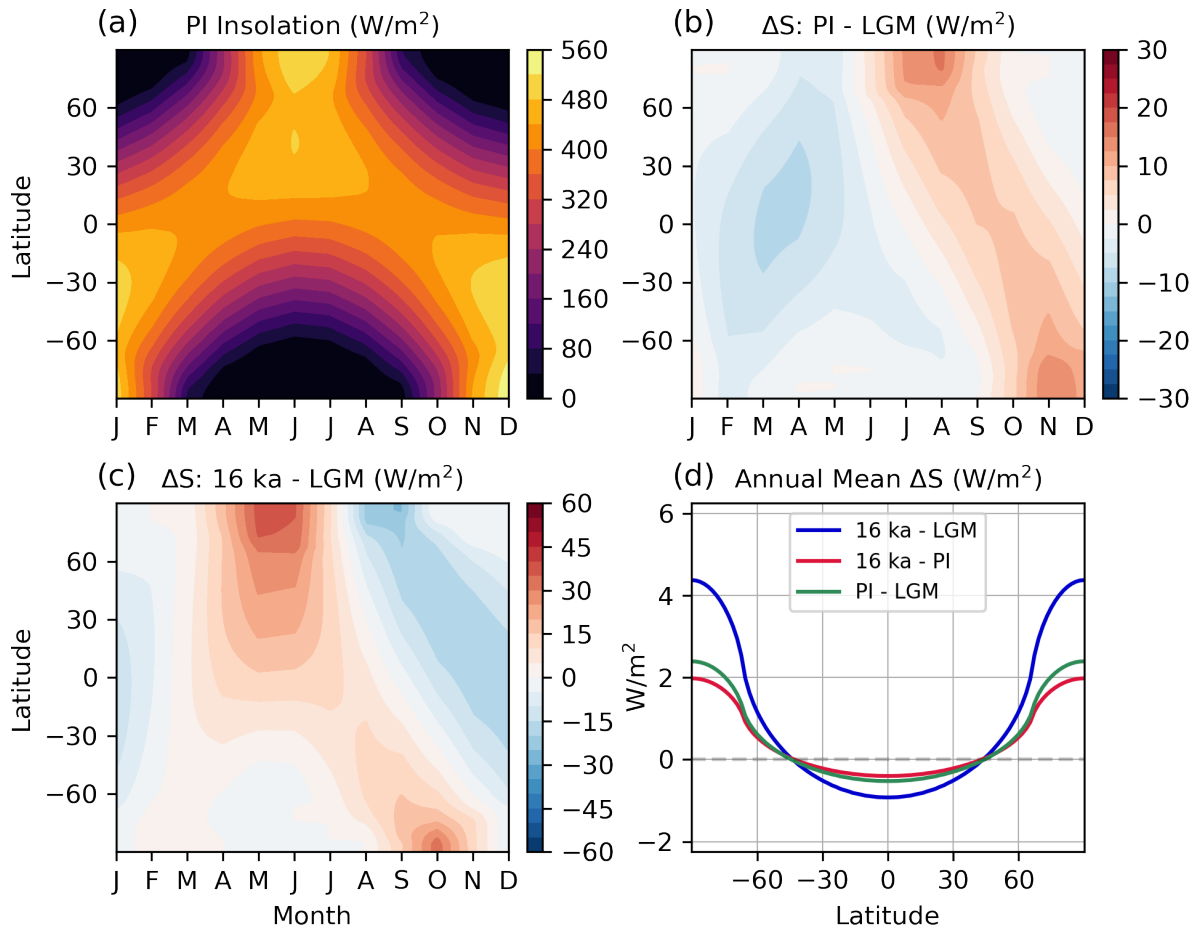

Figure S11. (a) Insolation as a function of season and latitude in the preindustrial simulation. (b) Difference in insolation between PI and LGM. (c) As in (b), but for the difference between 16 ka and LGM. (d) Zonal-mean insolation differences between 16 ka and LGM, 16 ka and PI, and PI and LGM, reflecting differences in obliquity. Vernal equinox is defined as March 21st at noon for all experiments.

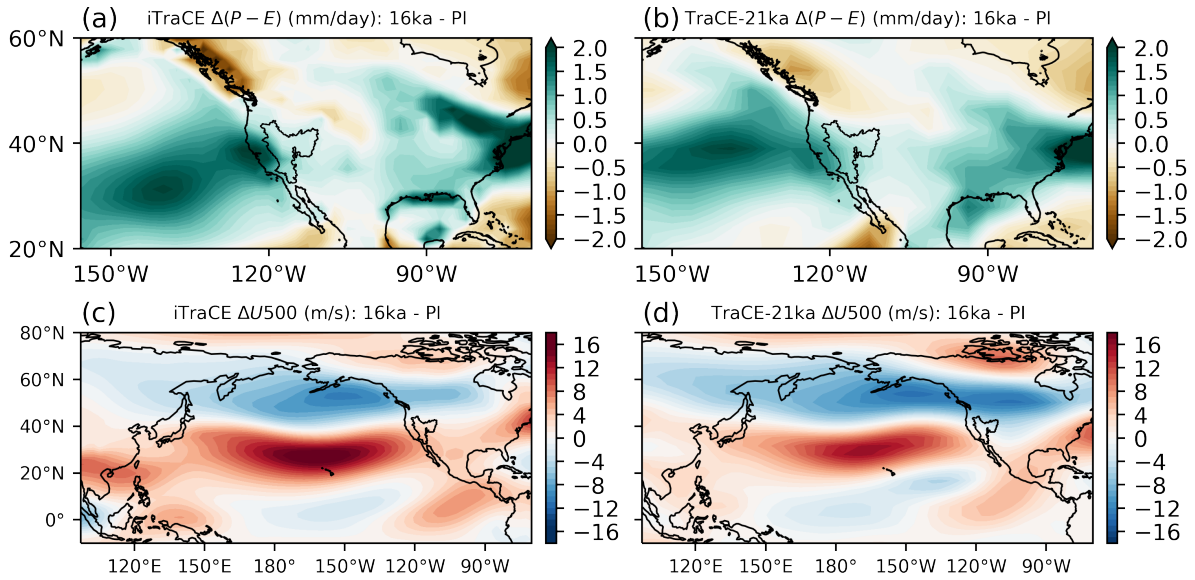

Figure S12. Difference in $(P - E)$ and North Pacific atmospheric circulation between 16 ka and PI. (a) Difference in $(P - E)$ between 16 ka and PI for iTraCE. (b) as in (a), but for TraCE-21ka. (c) Difference in winter-mean (DJF) zonal velocity at 500 hPa (U500; m/s) between 16 ka and PI for iTraCE. (d) as (c), but for TraCE-21ka.

References

Lüthi, D., Le Floch, M., Bereiter, B., Blunier, T., Barnola, J.-M., Siegenthaler, U., ... others (2008). High-resolution carbon dioxide concentration record 650,000–800,000 years before present. *nature*, *453*(7193), 379–382.

Monnin, E., Indermuhle, A., Dallenbach, A., Fluckiger, J., Stauffer, B., Stocker, T. F., ... Barnola, J.-M. (2001). Atmospheric CO_2 concentrations over the last glacial termination. *science*, *291*(5501), 112–114.

Peltier, W. R., Argus, D., & Drummond, R. (2015). Space geodesy constrains ice age terminal deglaciation: The global ice-6g_c (vm5a) model. *Journal of Geophysical Research: Solid Earth*, *120*(1), 450–487.